RSC Advances

PAPER

View Article Online
View Journal | View Issue

Cite this: *RSC Adv.*, 2019, **9**, 20618

La_2O_3-coated $Li_2ZnTi_3O_8$@C as a high performance anode for lithium-ion batteries†

Zhaohui Meng,[a] Suhong Wang,[a] Hongwei Wang,[a] Lijuan Wang *[b] and Song Wang*[b]

Received 22nd May 2019
Accepted 27th June 2019

DOI: 10.1039/c9ra03846a

rsc.li/rsc-advances

$Li_2ZnTi_3O_8C@La_2O_3$ (LZTO@C@La_2O_3) coated with composite protective layers is successfully fabricated *via* a facile solid-state route. The co-coating strategy greatly improves the electrochemical performance of LZTO. 89.8%, 77.2% and 76.7% of the discharge specific capacities for the 2nd cycle can be retained at the 200th cycle at 1, 2 and 3 A g^{-1}, respectively. At 4 and 5 A g^{-1}, 174.3 and 166.1 are still retained for the 100th cycle, respectively. Even at a high temperature of 55 °C, LZTO@C@La_2O_3 still has good cycling performance. The excellent electrochemical performance is due to the stable surface structure between LZTO and the electrolyte, a good conductive network, small particle size, and large specific surface area as well as pore volume.

Introduction

Lithium-ion batteries (LIBs) have been widely used in portable electronics and considered as promising power sources for hybrid electric vehicles (HEVs) as well as electric vehicles (EVs) since they were commercialized in the early 1990s.[1,2] In commercial LIBs, graphite is the main anode material. However, the carbon material suffers from poor rate capability and safety originating from the formation of lithium dendrites owing to its low Li-intercalation potential close to 0 V (*vs.* Li/Li^+).[3] To solve these problems, the spinel $Li_4Ti_5O_{12}$ (LTO) with good rate capability and safety, has been developed as a new commercial candidate.[4] Nevertheless, its small theoretical specific capacity (175 mA h g^{-1}) restricts it from being widely used in LIBs with high energy density. Therefore, many new anode materials with large specific capacities, including metallic oxides,[5–9] alloy compounds[10–12] and Si-based materials,[13,14] have been researched. Unfortunately, the large volume expansion severely deteriorates the cycling performance of the materials mentioned above. So, it is urgent to find an anode material with good safety, acceptable specific capacity and small volume change.

In recent, spinel structure $Li_2ZnTi_3O_8$ (LZTO) with the space group of $P4_332$ has received much attention as an appealing anode for various advantages:[15–19] (1) the main Li-intercalation potential is *ca.* 0.5 V which can prevent the growth of the dendritic lithium and ensure the good safety for LZTO. (2) Compared with the theoretical specific capacity of LTO, the value of LZTO (229 mA h g^{-1}) increases by 30%. (3) Similar to LTO, the LZTO shows zero volume change which can benefit the cyclic performance. (4) The three-dimensional network constructed by LiO_6 and TiO_6 octahedrons is beneficial to Li^+ diffusion. (5) The preparation of LZTO is low cost, simpleness and environment friendly, so it is proper for large-scale production.

Even so, the low electronic conductivity of LZTO results in its poor rate capability. Many methods have been adopted to solve the problem, such as synthesizing nano-sized LZTO,[20,21] coating conductive agents[22,23] and doping with metal ions.[24–27] The rate capability of LZTO has been improved *via* the three ways above. Moreover, LZTO has good cyclic performance as a zero-strain material theoretically. In fact, its cyclic performance is unsatisfactory due to the dissolution of transition metal elements in LZTO attacked by HF from the lithium salt $LiPF_6$ in the electrolyte. Surface coating has been considered as an effective method of solving the issue.[28–31] Tang *et al.*[29] synthesized $Li_2ZnTi_3O_8/La_2O_3$ with good cyclic performance. Nevertheless, the rate capability of $Li_2ZnTi_3O_8/La_2O_3$ should be greatly improved. At 3 A g^{-1}, its discharge specific capacity is only 149.3 mA h g^{-1}.

Herein, we firstly report the fabrication of $Li_2ZnTi_3O_8$@C@La_2O_3 co-coated with carbon and La_2O_3 by a simple solid-state route using nitrilotriacetic acid (NTA) as the carbon source (Fig. 1). The electronic conductivity can be greatly enhanced due to the existence of carbon, which will benefit its rate capability. The carbon and La_2O_3 as co-coating layers can suppress the dissolution of the surface metal ions from LZTO and then improve the cyclic performance.

Experimental

Synthesis of $Li_2ZnTi_3O_8$@C@La_2O_3 and $Li_2ZnTi_3O_8$@C

The $Li_2ZnTi_3O_8$@C@La_2O_3 anode was fabricated by a two-step solid-state route. Li_2CO_3, ZnO, TiO_2 and NTA were dispersed in ammonium hydroxide (9 wt%) and ball-milled for 5 h in the molar ratio of 1.1 : 1 : 3 : 2. The Li salt can volatilize in sintering

[a]College of Chemistry and Pharmaceutical Engineering, Nanyang Normal University, Nanyang 473061, China

[b]School of Chemistry and Material Science, Liaoning Shihua University, Fushun 113001, Liaoning, China. E-mail: lijuanw123@163.com; Tel: +86-24-56861711

† Electronic supplementary information (ESI) available. See DOI: 10.1039/c9ra03846a

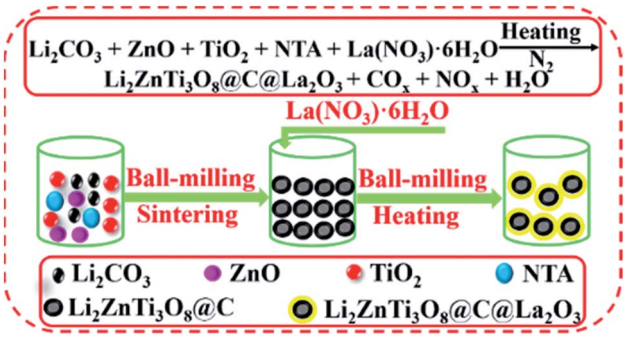

Fig. 1 Schematic illustration for the synthetic process of the LZTO@C@La_2O_3 anode.

process at high temperature. So, the Li source is slight excess. The mixture was dried at 90 °C and then sintered at 700 °C for 3 h in N_2. The obtained product was ball-milled with $La(NO_3)_3 \cdot 6H_2O$ for 5 h with the mass ratio of 1 : 0.0935. The mixture was dried at 90 °C and then heated at 550 °C for 3 h in N_2. The obtained material was denoted as $Li_2ZnTi_3O_8$@C@La_2O_3 (LZTO@C@La_2O_3). The same processes were used to synthesize $Li_2ZnTi_3O_8$@C (LZTO@C) without $La(NO_3)_3 \cdot 6H_2O$ and post-treatment at 550 °C for 3 h in N_2.

Physical and electrochemical performance measurements

The detailed measurements were shown in ESI.†

Results and discussion

The diffraction peaks of LZTO@C and LZTO@C@La_2O_3 can be well attributed to the spinel LZTO (JCPDS# 86-1512) (Fig. 2a), indicating that the crystal structure of LZTO is not altered in the existence of carbon and La_2O_3. The lattice parameters of LZTO@C@La_2O_3 are slightly larger than those of LZTO@C (Table S1†) due to the extra post-treatment at 550 °C for 3 h in N_2 for LZTO@C@La_2O_3. Moreover, the diffraction peaks of LZTO@C@La_2O_3 have no apparent shift in contrast with the patterns of LZTO@C (Fig. 2a and b). These indicate that the La element is not doped into the crystal lattice but coated on the surface of LZTO particles in the form of La_2O_3. The XPS data further confirm that the La element exists in the form of La_2O_3 in LZTO@C@La_2O_3 (Fig. S1a and b†). The content of La_2O_3 is *ca.* 3 wt% in LZTO@C@La_2O_3 calculated from the ICP result. However, there are no diffraction peaks related to La_2O_3 are observed. It is possible that the content of La_2O_3 is low or the La_2O_3 coating layer is thin. The XPS spectra show that there is carbon in LZTO@C and LZTO@C@La_2O_3 (Fig. S1a, c and d†). The carbon content is *ca.* 11.5 wt% for LZTO@C and LZTO@C@La_2O_3 (Fig. S2†). Nevertheless, the carbon is not detected from the XRD results. It may be that the carbon is amorphous.[32,33] The superficial electronic conductivity of LZTO can be greatly enhanced due to the existence of carbon. The carbon and La_2O_3 co-coating layers can prevent the direct contact between LZTO and electrolyte, and then some side reactions can be weakened on the interface.

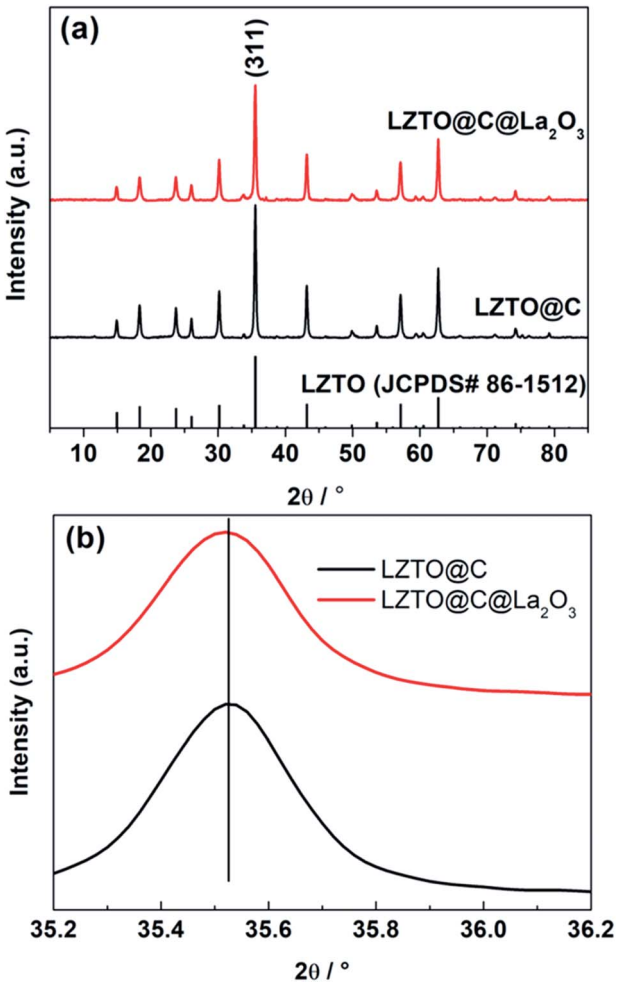

Fig. 2 (a) X-ray diffraction patterns and (b) magnified (311) peaks of the LZTO@C and LZTO@C@La_2O_3 anodes.

The LZTO@C particles are interconnected to each other. However, some of them are aggregated together marked by the circle (Fig. 3a). The LZTO@C@La_2O_3 is agglomerates of tiny particles (Fig. 3b). There is carbon in LZTO@C and LZTO@C@La_2O_3 from the TEM images and the EDX results (Fig. 3c–f and S3†). Compared with LZTO@C, the LZTO@C@La_2O_3 particles can be more homogeneously coated (Fig. 3e and f). La element is also investigated from EDX spectroscopy and uniformly dispersed onto the LZTO@C@La_2O_3 (Fig. S3†). The HRTEM image further indicates that the La element in the form of La_2O_3 exists in LZTO@C@La_2O_3 (Fig. 3h). Compared with LZTO@C, the carbon and La_2O_3 co-coating layers make LZTO@C@La_2O_3 have smaller particle size of 36 nm and then larger specific surface area of 72.8 $m^2\ g^{-1}$ (Fig. S3j, k, S4 and Table S2†), which can increase the contact area between LZTO@C@La_2O_3 particles and electrolyte, and then will improve the reversible capacity. In addition, LZTO@C@La_2O_3 has larger total pore volume and average pore diameter in contrast with LZTO@C (Fig. S4 and Table S2†). The small particle size and large pore can speed the diffusion of Li^+

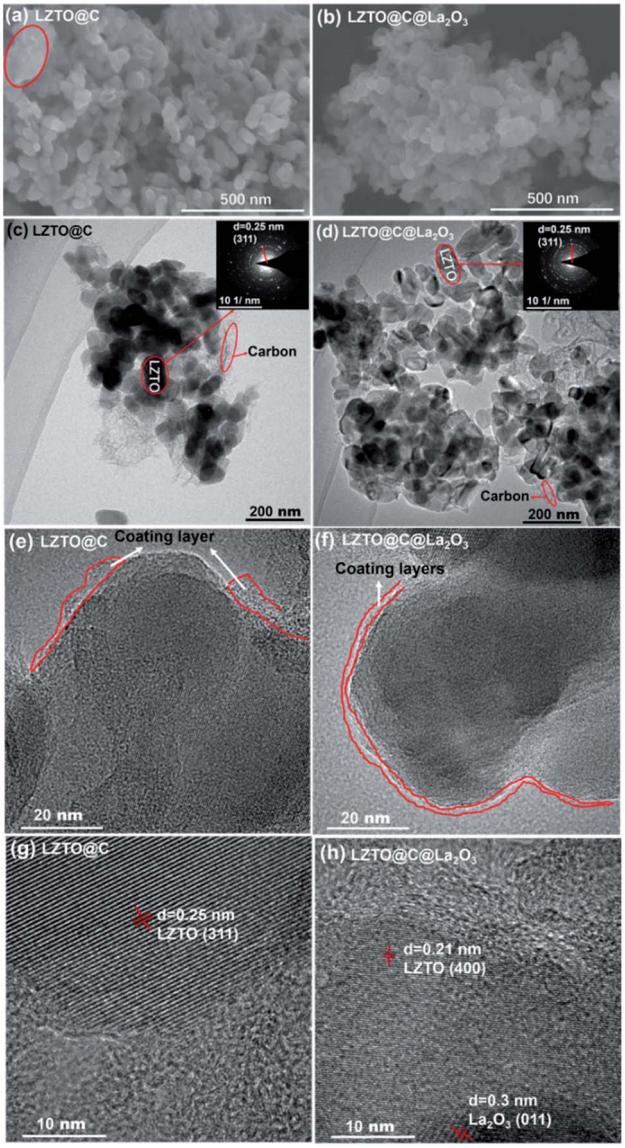

Fig. 3 SEM images of (a) LZTO@C and (b) LZTO@C@La_2O_3; (c and e) TEM images of LZTO@C at different magnifications; (d and f) TEM images of LZTO@C@La_2O_3 at different magnifications; HRTEM images of (g) LZTO@C and (h) LZTO@C@La_2O_3. Selected area electron diffraction (SAED) patterns (inset, upper-right corner of (c) and (d)).

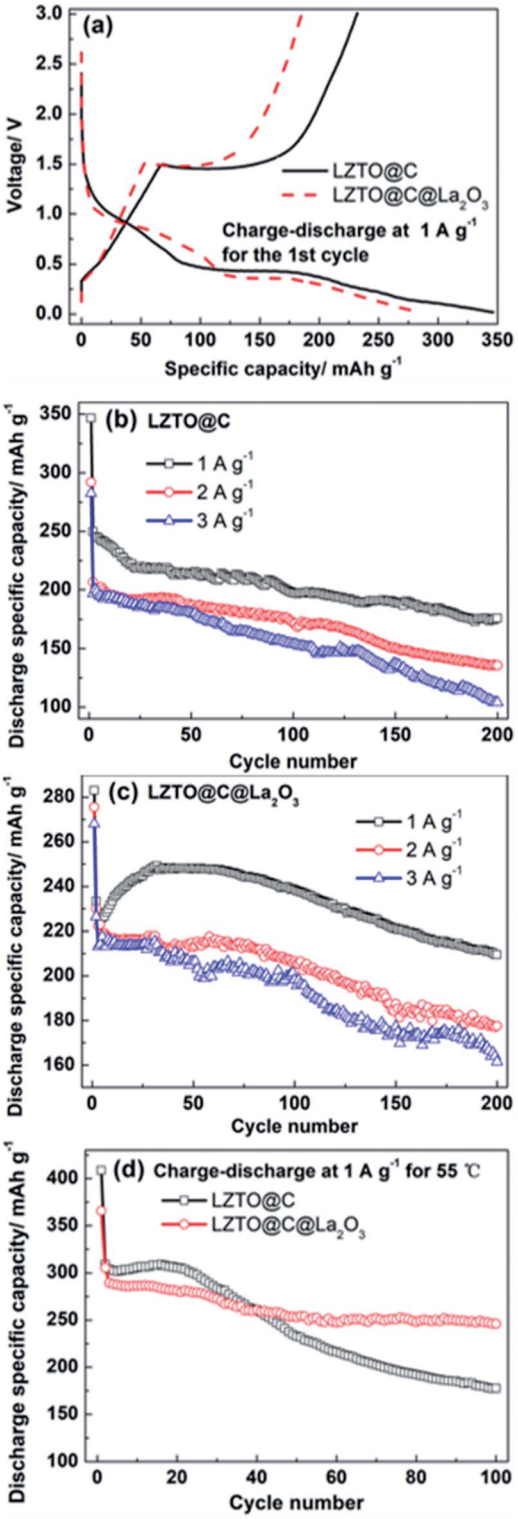

Fig. 4 (a) The charge–discharge curves at the 1st cycle of LZTO@C and LZTO@C@La_2O_3; cyclic performance of (b) LZTO@C and (c) LZTO@C@La_2O_3 at 1, 2 and 3 A g^{-1} in 0.02–3.0 V; (d) cyclic performance of LZTO@C and LZTO@C@La_2O_3 at 1 A g^{-1} for 55 °C in 0.02–3.0 V.

ions and then will benefit the rate capability of LZTO@C@La_2O_3.

The initial galvanostatic charge–discharge profiles are depicted in Fig. 4a at 1 A g^{-1} in 0.02–3 V for LZTO@C and LZTO@C@La_2O_3. For the two samples, there is a charge plateau at *ca.* 1.45 V and two discharge plateaus at *ca.* 1.03 and 0.42 V on the curves with two-step intercalation of Li^+ ions, based on the Ti^{4+}/Ti^{3+} redox couple.[24] The electrochemical reaction mechanisms were also confirmed *via* the cyclic voltammetry (CV) measurements (Fig. S5 and Table S3†). The one anodic peak and two cathodic peaks correspond to the one charge plateau and two discharge plateaus for the two samples, respectively. Compared with LZTO@C@La_2O_3, the discharge specific capacity (346.5 mA h g^{-1}) is larger and the coulombic efficiency (67%) is higher for LZTO@C at the 1st cycle (Table 1). The poor electrochemical performance of LZTO@C@La_2O_3 at the 1st cycle is owing to the following reasons: (1) the specific capacity

Table 1 Discharge capacities and coulombic efficiency of LZTO@C and LZTO@C@La_2O_3 for the 1st cycle at 1 A g^{-1}

Samples	Discharge specific capacity (mA h g^{-1})	Coulombic efficiency
LZTO@C	346.5	67%
LZTO@C@La_2O_3	283	65.4%

is calculated based on the mass of LZTO@C@La_2O_3. The mass ratio of La_2O_3 is *ca.* 3 wt%. The existence of inactive La_2O_3 lowers the specific capacity of LZTO@C@La_2O_3. (2) The La_2O_3 coating layer increases the resistance of LZTO@C@La_2O_3/Li (Fig. S6 and Table S4†). The polarization increases during insertion and deinsertion of Li^+ ions (Fig. S5 and Table S3†). However, LZTO@C@La_2O_3 has larger specific capacities in contrast with LZTO@C after 11 cycles at 1 A g^{-1} (Fig. 4b and c). It is because the internal resistance and polarization decrease for the LZTO@C@La_2O_3/Li in the subsequent cycling process (Fig. S7†), and then the diffusion paths of Li^+ ions become smooth. At the 200th cycle, the capacity retention is 70.5% and 89.8% corresponding to the 2nd cycle for LZTO@C and LZTO@C@ La_2O_3, respectively (Table 2).

Compared with LZTO@C, LZTO@C@La_2O_3 has smaller initial discharge specific capacities but better cyclic performance at 2 and 3 A g^{-1} (Fig. 4b, c and Table 2). After 200 cycles, the capacity retention based on the 2nd cycle is 77.2% and 76.7% for LZTO@C@La_2O_3 at 2 and 3 A g^{-1}, respectively. The retention is 65.7% and 52.8% for LZTO@C at 2 and 3 A g^{-1}, respectively. At 55 °C, the LZTO@C@La_2O_3 still has better cyclic performance (Fig. 4d). After 100 cycles, 57.5% and 80.6% of the capacities for the 2nd cycle can be kept for LZTO@C and LZTO@C@La_2O_3, respectively. Its cyclic performance exceeds many previous reports (Table S5†). The enhanced cyclic performance for LZTO@C@La_2O_3 is attributed to the following reasons: (1) there is some HF in the commercial electrolyte. It can result in the dissolution of transition metal elements for the LZTO electrode, leading to capacity decay.[34,35] The carbon and La_2O_3 co-coating layers can prevent LZTO directly contacting with electrolyte. In addition, La_2O_3 can react with HF. These can weaken the attract from HF to active material LZTO. The mechanism is shown in Fig. S8† in detail. (2) The integrity of LZTO@C@La_2O_3 electrode can be well kept and good electrical contact can be obtained during cycling process (Fig. S9b and d†).

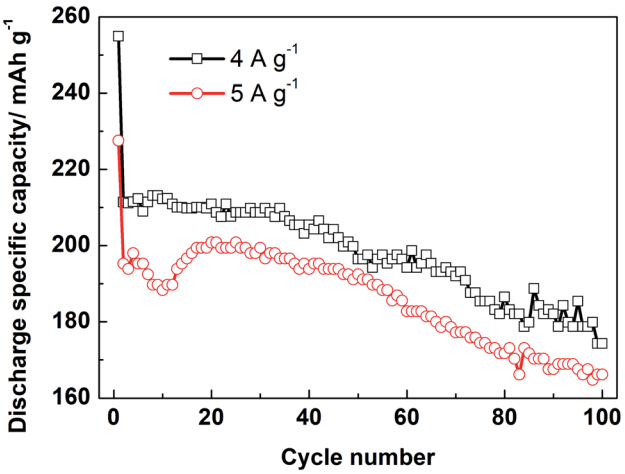

Fig. 5 Cyclic performance of LZTO@C@La_2O_3 at 4 and 5 A g^{-1} in 0.02–3.0 V.

Moreover, the LZTO@C@La_2O_3 exhibits good rate capability. The discharge specific capacities are 211.4 and 195.3 mA h g^{-1} at 4 and 5 A g^{-1} for the 2nd cycle, respectively. Cycling for 100 cycles, 174.3 and 166.1 mA h g^{-1} are still kept, respectively (Fig. 5). Its rate capability exceeds many previous reports (Table S6†), which may be due to the reasons below: (1) the carbon coating layer can enhance the superficial electronic conductivity of LZTO. (2) The existence of carbon and La_2O_3 co-coating layers makes LZTO have small particle size, large specific surface area and pore size. (3) The presence of carbon and La_2O_3 makes good adhesion between LZTO and Cu current collector and then good conductive network is formed (Fig. S9b–d†).

The cyclic data of LZTO@C and LZTO@C@La_2O_3 at different current densities are exhibited in Fig. 6. Compared with LZTO@C, LZTO@C@La_2O_3 has smaller initial discharge specific capacity at low current density of 0.4 A g^{-1}. However, discharge specific capacities of LZTO@C@La_2O_3 exceed those of LZTO@C at different current densities in the subsequently cycling process. The discharge specific capacities are *ca.* 280 and 315 mA h g^{-1} for LZTO@C and LZTO@C@La_2O_3 at 0.4 A g^{-1}, respectively. When the current density was reset to 0.4 A g^{-1} after cycling for 60 cycles at different current densities, *ca.* 285 and 325 mA h g^{-1} are obtained for LZTO@C and LZTO@C@La_2O_3, respectively. Good cyclic reversibility is obtained for the two samples. In addition, the two electrodes are

Table 2 Discharge specific capacities and capacity retention at the 200th cycle for 1, 2 and 3 A g^{-1} based on the 2nd cycle of LZTO@C and LZTO@C@La_2O_3

	LZTO@C		LZTO@C@La_2O_3	
Current density (A g^{-1})	Specific capacity (mA h g^{-1})	Capacity retention	Specific capacity (mA h g^{-1})	Capacity retention
1	249.7	70.5%	233.4	89.8%
2	206.7	65.7%	230.2	77.2%
3	196.9	52.8%	210.6	76.7%

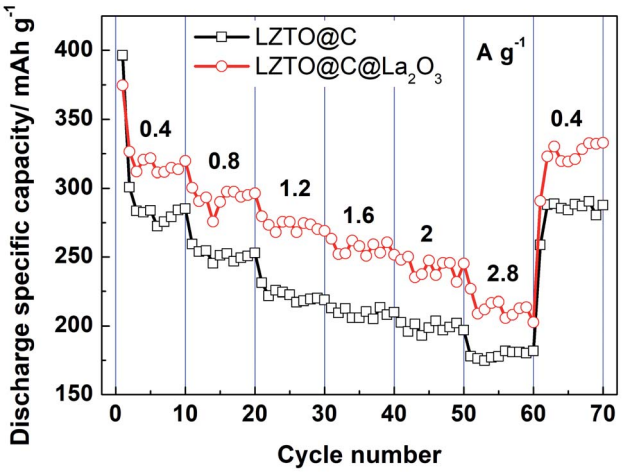

Fig. 6 Cyclic performance of LZTO and LZTO@C@La_2O_3 at different current densities.

activated after cycling at 0.4 A g^{-1},[26] so large capacities are obtained in the subsequent cycling process.

Conclusions

$Li_2ZnTi_3O_8$@C@La_2O_3 co-coated with carbon and La_2O_3 has been successfully fabricated *via* a simple solid-state route. The carbon can improve the electronic conductivity, which benefits its rate capability. The carbon and La_2O_3 co-coating layers can suppress the dissolution transition metal elements and then greatly improve the cyclic performance. In addition, the co-coating layers make LZTO have large specific surface area as well as pore size, and make LZTO@C@La_2O_3 electrode form good conductive network, which can improve its electrochemical performance. The designed LZTO@C@La_2O_3 composite material exhibits good cyclic performance and high rate capability. In consideration of the facile synthetic route and remarkable electrochemical performance, LZTO@C@La_2O_3 coated with composite protective layers is thought to be a promising anode of LIBs.

Conflicts of interest

There are no conflicts to declare.

Acknowledgements

We thank for the support from the Henan Joint Funds of the National Natural Science Foundation of China (U1504532) and the Natural Science Foundation of Liaoning Shihua University (2018XJJ-012).

Notes and references

1 D. Chen, Z. Lou, K. Jiang and G. Shen, *Adv. Funct. Mater.*, 2018, **28**, 1805596.
2 T. Kim, W. Song, D.-Y. Son, L. K. Ono and Y. Qi, *J. Mater. Chem. A*, 2019, **7**, 2942–2964.
3 M. Salah, P. Murphy, C. Hall, C. Francis, R. Kerr and M. Fabretto, *J. Power Sources*, 2019, **414**, 48–67.
4 C. Han, Y.-B. He, M. Liu, B. Li, Q.-H. Yang, C.-P. Wong and F. Kang, *J. Mater. Chem. A*, 2017, **5**, 6368–6381.
5 H. Chen, J. He, Y. Li, S. Luo, L. Sun, X. Ren, L. Deng, P. Zhang, Y. Gao and J. Liu, *J. Mater. Chem. A*, 2019, **7**, 7691–7700.
6 S. Jia, Y. Wang, X. Liu, S. Zhao, W. Zhao, Y. Huang, Z. Li and Z. Lin, *Nano Energy*, 2019, **59**, 229–236.
7 Q. Feng, H. Li, Z. Tan, Z. Huang, L. Jiang, H. Zhou, H. Pan, Q. Zhou, S. Ma and Y. Kuang, *J. Mater. Chem. A*, 2018, **6**, 19479–19487.
8 W. Zhang, Y. Fu, W. Liu, L. Lim, X. Wang and A. Yu, *Nano Energy*, 2019, **57**, 48–56.
9 T. Herdt, D. Deckenbach, M. Bruns and J. J. Schneider, *Nanoscale*, 2019, **11**, 598–610.
10 W. Qi, J. G. Shapter, Q. Wu, T. Yin, G. Gao and D. Cui, *J. Mater. Chem. A*, 2017, **5**, 19521–19540.
11 K.-H. Nam, G.-K. Sung, J.-H. Choi, J.-S. Youn, K.-J. Jeon and C.-M. Park, *J. Mater. Chem. A*, 2019, **7**, 3278–3288.
12 Z. Yi, Z. Wang, Y. Cheng and L. Wang, *Energy Environ. Mater.*, 2018, **1**, 132–147.
13 Y. Son, J. Ma, N. Kim, T. Lee, Y. Lee, J. Sung, S. H. Choi, G. Nam, H. Cho, Y. Yoo and J. Cho, *Adv. Energy Mater.*, 2019, **9**, 1803480.
14 K. Feng, M. Li, W. Liu, A. G. Kashkooli, X. Xiao, M. Cai and Z. Chen, *Small*, 2018, **14**, 1702737.
15 Z. Hong, X. Zheng, X. Ding, L. Jiang, M. Wei and K. Wei, *Energy Environ. Sci.*, 2011, **4**, 1886.
16 H. Tang, Q. Weng and Z. Tang, *Electrochim. Acta*, 2015, **151**, 27–34.
17 L. Wang, L. Wu, Z. Li, G. Lei, Q. xiao and P. Zhang, *Electrochim. Acta*, 2011, **56**, 5343–5346.
18 X. Li, L. Wang, C. Li, B. Chen, Q. Zhao and G. Zhang, *J. Power Sources*, 2016, **308**, 65–74.
19 X. Li, Q. Xiao, B. Liu, H. Lin and J. Zhao, *J. Power Sources*, 2015, **273**, 128–135.
20 Z. Hong, M. Wei, X. Ding, L. Jiang and K. Wei, *Electrochem. Commun.*, 2010, **12**, 720–723.
21 L. Wang, Z. Meng, H. Wang, X. Li and G. Zhang, *Ceram. Int.*, 2016, **42**, 16872–16881.
22 C. Chen, C. Ai, X. Liu, Y. He, S. Yang and Y. Wu, *J. Alloys Compd.*, 2017, **698**, 692–698.
23 Z. Meng, L. Wang, X. Li, G. Zhang and H. Li, *Int. J. Hydrogen Energy*, 2017, **42**, 2177–2186.
24 C. Chen, C. Ai, X. Liu and Y. Wu, *Electrochim. Acta*, 2017, **227**, 285–293.
25 H. Li, Z. Li, X. Liang, J. Ouyang, Y. Ma, Y. Cui, C. Ma and Z. Tang, *Mater. Lett.*, 2017, **192**, 128–132.
26 S. Wang, Y. Bi, L. Wang, Z. Meng and B. Luo, *Electrochim. Acta*, 2019, **301**, 319–324.
27 T.-F. Yi, J.-Z. Wu, J. Yuan, Y.-R. Zhu and P.-F. Wang, *ACS Sustainable Chem. Eng.*, 2015, **3**, 3062–3069.
28 Z. Li, H. Li, Y. Cui, Z. Du, Y. Ma, C. Ma and Z. Tang, *J. Alloys Compd.*, 2017, **692**, 131–139.

29 H. Tang, L. Zan, J. Zhu, Y. Ma, N. Zhao and Z. Tang, *J. Alloys Compd.*, 2016, **667**, 82–90.
30 H. Yang, X.-H. Wang, Y.-X. Qi, N. Lun, Y.-M. Cao and Y.-J. Bai, *ACS Sustainable Chem. Eng.*, 2017, **5**, 6099–6106.
31 H. Tang, J. Zhu, C. Ma and Z. Tang, *Electrochim. Acta*, 2014, **144**, 76–84.
32 C. Chen, C. Ai, Y. He, S. Yang and Y. Wu, *J. Alloys Compd.*, 2017, **705**, 438–444.
33 Y. Ren, P. Lu, X. Huang, J. Ding and H. Wang, *RSC Adv.*, 2016, **6**, 49298–49306.
34 H. Tang, Y. Zhou, L. Zan, N. Zhao and Z. Tang, *Electrochim. Acta*, 2016, **191**, 887–894.
35 H. Tang, L. Zan, W. Mao and Z. Tang, *J. Electroanal. Chem.*, 2015, **751**, 57–64.